IEEE Access
Multidisciplinary ⋮ Rapid Review ⋮ Open Access Journal

Received 20 July 2025, accepted 8 September 2025, date of publication 25 September 2025, date of current version 9 October 2025.

Digital Object Identifier 10.1109/ACCESS.2025.3614293

RESEARCH ARTICLE

A Wireless and Machine Learning-Based Electrochemical Biosensor Potentiostat System for CD63 Protein Detection in Lung Cancer Biomarkers

AHMED FAOZI RABEA[1], EFFARIZA HANAFI[1], (Senior Member, IEEE), SUBHASHINI RAJ KUMAL[2,3], ANIS SALWA MOHD KHAIRUDDIN[1], (Member, IEEE), AND LEO BEY FEN[2,4]

[1]Department of Electrical Engineering, Faculty of Engineering, Universiti Malaya, Kuala Lumpur 50603, Malaysia
[2]Department of Molecular Medicine, Faculty of Medicine, Universiti Malaya, Kuala Lumpur 50603, Malaysia
[3]Department of Medical Microbiology, Faculty of Medicine, Universiti Malaya, Kuala Lumpur 50603, Malaysia
[4]Nanotechnology and Catalysis Research Centre (NANOCAT), Universiti Malaya, Kuala Lumpur 50603, Malaysia

Corresponding authors: Effariza Hanafi (effarizahanafi@um.edu.my) and Anis Salwa Mohd Khairuddin (anissalwa@um.edu.my)

This work was supported by the Universiti Malaya Impact Oriented Interdisciplinary Research Grant (IIRG) Program under Grant IIRG002C-2021FNW and Grant IIRG002B-2021FNW.

ABSTRACT Lung cancer remains one of the leading causes of cancer-related deaths globally, with approximately 2.5 million new cases and 1.8 million deaths reported annually according to World Health Organization in 2022. Early and accurate detection is crucial for improving survival rates through timely treatment. However, current detection methods face challenges such as invasiveness, high costs, and delayed diagnosis. Electrochemical biosensors, which use potentiostats to detect biological analytes by controlling cell voltage and measuring current, voltage, or impedance, offer a rapid and sensitive alternative. Nevertheless, many existing potentiostats are limited by narrow voltage ranges, single current measurement capabilities, and inadequate support for advanced electrochemical techniques. This study presents a novel wireless electrochemical biosensor potentiostat system enhanced with machine learning and Internet of Things (IoT) integration for the detection of lung cancer biomarkers, specifically the CD63 protein. The system is designed to be portable, energy efficient, cost-effective, and high sensitive, supporting advanced electrochemical techniques such as cyclic voltammetry (CV) and square wave voltammetry (SWV). It achieves a limit of detection (LoD) of 2×10^1 particles/mL and a sensitivity of 5.188 μA per log concentration unit, comparable to the commercial systems like uStat8000 potentiostat. Furthermore, the integrated random forest classifier enables fast and automated data interpretation, achieving accuracy rates of 83.5% and 87.5% for CV and SWV cases, respectively. Overall, the developed platform offers a smart, portable, and scalable solution for point-of-care diagnostics, contributing to early detection and improved prognosis in lung cancer management.

INDEX TERMS Biosensor, biomarkers, electrochemical, lung cancer, machine learning.

I. INTRODUCTION

Cancer is an inherently intricate and exceedingly diverse ailment that is frequently distinguished by the uncontrolled and rapid division and proliferation of cells. This complicated illness is considered the leading source of death globally, with around 20 million new cases and 9.7 million deaths every year according to World Health Organization (WHO) in 2022 [1]. Due to its pervasive nature, susceptibility to recurrence despite treatment, substantial morbidity and mortality, and

The associate editor coordinating the review of this manuscript and approving it for publication was Norbert Herencsar.

other factors, cancer has been the focus of extensive scientific investigation in recent decades [2].

Lung cancer in particular is a complex disease with multiple subtypes, and its incidence varies globally. According to the International Agency for Research on Cancer (IARC) [3], in 2022, there were approximately 2.5 million new cases of lung cancer worldwide, accounting for nearly 12.4 percentage of all cancer cases. Furthermore, lung cancer mortality rates are alarmingly high, with approximately 1.8 million deaths in the same year.

Early and accurate cancer identification is essential for enabling prompt treatment and increasing patient survival rates since most treatment approaches work better on smaller tumors. The efficacy of traditional approaches in identifying early lung neoplasms is limited due to their reliance on morphological criteria. Conventional procedures include chemotherapeutical, X-ray, and optical coherence exhibit several drawbacks including comparatively sluggishness, labor-intensiveness, time-consuming, the requirement for sophisticated equipment, and expensive diagnostic tests [4]. Various approaches, including electrochemistry, electrochemiluminescence (ECL), and low-cost biomarker detection techniques, have been used to date for biomarker identification [5].

Biosensors have emerged as promising platforms for rapid and sensitive diagnostics. They offer advantages such as high sensitivity, specificity, and real-time analysis capabilities. The main working concept of the biosensor is by translating signals from biological molecule interactions into a detectable signal that can be measured as an observable output. Biosensors are used to identify and measure specific biological markers or analytes (such as proteins, DNA, RNA, and cells). Biosensor types are broadly classified based on the transduction mechanism employed. Electrochemical biosensors measure changes in electrical properties such as current, voltage, or resistance while optical biosensors utilize light-based techniques, such as fluorescence, absorbance, or refractive index changes. Additionally, the piezoelectric biosensors exploit the change in mass or frequency of a piezoelectric crystal. Figure 1 illustrates various components of a biosensor. The electrochemical biosensors rely on the concept of the potentiostat, a vital component of electrochemical measurement systems [6]. Potentiometry, amperometry or voltammetry, and impedance spectroscopy are among the sophisticated techniques that fall under the general category of electrochemical biosensors [7].

A potentiostat is an electronic device used to control and measure the potential difference between a working electrode and a reference electrode, while maintaining a constant potential at the working electrode. It achieves this by applying a specific voltage to the working electrode, which is the electrode where the electrochemical reaction of interest occurs. The reference electrode provides a stable potential against which the working electrode's potential is measured and controlled. A counter electrode completes

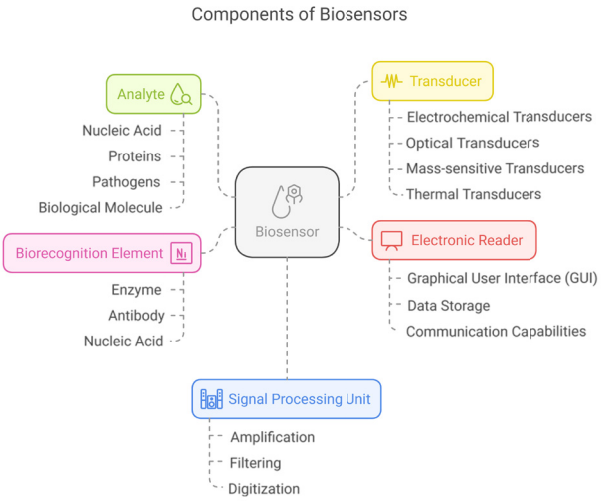

FIGURE 1. Biosensors structure.

the circuit and allows current flow. In the context of electrochemical biosensing, the potentiostat enables the detection of biomolecular interactions occurring at the electrode surface. By applying a potential to the working electrode and measuring the resulting current or impedance changes, the potentiostat allows for the quantitative analysis of biomarkers [8]. Biomarkers are very relevant molecules for therapy that undergo significant alterations during the propagation of cancer. Biomarkers include proteins, metabolites, isoenzymes, nucleic acids, and hormones. In the case of lung cancer biomarker detection, when a sample containing lung cancer biomarkers is introduced to the electrochemical biosensor, the biomarkers bind to the immobilized antibodies or aptamers, leading to measurable changes in the electrical properties of the electrode surface which then can be measured by the potentiostat [9].

In recent years, the integration of machine learning (ML) techniques into electrochemical potentiostat systems has emerged as a powerful approach to enhance the diagnostic capabilities of biosensors [10]. By enabling automated analysis of complex electrochemical data, ML algorithms can significantly improve the sensitivity, specificity, and overall reliability of biomarker detection. These techniques can identify subtle patterns and trends within voltammetric signals that may not be easily discernible through traditional analytical methods. In the context of biosensor-based diagnostics, ML models such as Random Forest, Support Vector Machine, and k-Nearest Neighbors can be trained using features extracted from raw electrochemical measurements (e.g., peak current, potential, signal shape, and area under the curve) to classify the presence or absence of disease-specific biomarkers. Once trained, the models can be embedded directly into the system's processing unit or interfaced via a graphical user interface (GUI),

allowing real-time interpretation of biosensor responses. This integration transforms conventional potentiostats into intelligent diagnostic tools capable of providing rapid, data-driven decision support without the need for expert interpretation, which is particularly valuable in point-of-care or resource-limited settings [11]. Various studies have shown that artificial intelligence (AI) can enhance their selectivity and overall performance. Authors in [12] developed an innovative AI-supported voltammetric biosensor for the rapid, low-cost, and high-sensitivity detection of insulin and glucose in serum. Another study in [13] aimed to assist clinicians in decision-making and enhance the accuracy in detecting prostate cancer, particularly in ambiguous PI-RADS 3 lesions. PI-RADS is a scoring system used to assess the likelihood of prostate cancer in multiparameter magnetic resonance imaging and has a diagnostic accuracy of no more than 30–40%. The results revealed that AI algorithms successfully analyzed the sensor data from multiple biomarkers in conjunction with the PI-RADS score, increasing the diagnostic accuracy for prostate cancer in PI-RADS 3 patients from 30.4% to 66.7%. Graph-based deep learning has been applied to biomedical segmentation tasks that involve irregular, high-dimensional data structures, such as hand surface point cloud segmentation in rehabilitation contexts [14], [15].

Extracellular vesicles (EVs) are some promising examples of liquid biopsy biomarkers studied for cancer detection [16]. EVs can be categorized into exosomes, microvesicles or apoptotic bodies depending on their size, origin, morphology and buoyant density [17]. Exosomes are small EVs with sizes ranging from 30 to 150 nm in diameter and carry surface proteins such as TSG101, CD9, CD63, and CD81 give crucial information on the progress of cancer [18].

II. RELATED WORK AND CONTRIBUTION

Numerous electrochemical biosensors have been developed to sensitively detect lung cancer biomarkers. For instance, an aptasensor using gold and mesoporous nanoparticle-modified electrodes was designed to detect VEGF165 in lung cancer trials by measuring interactions between immobilized anti-VEGF165 aptamers and VEGF165, altering the electrode's interfacial properties. This aptasensor demonstrated high sensitivity in detecting trace VEGF levels in blood samples from lung cancer patients [19]. Similarly, a microfluidic system was developed to quantify the transmembrane protein CD63 using SWV, achieving a detection limit of 1×10^6 particles/mL [18]; however, further sensitivity enhancement still needed.

Another study [20] employed a double-antibody sandwich method with poly-enzyme signal amplification to quantify CD63 and CD81 in exosomes, showing potential for prostate cancer detection through reduced CD63-positive exosomes. In a separate work [21], Zhang et.al developed a DNA walker-based biosensor for detecting exosomal miRNA-21 reaching a detection limit of 67 μM, and potential for early cancer detection. Authors in [22] introduced an integrated assay device (iMEX) with eight-channel electrodes for multi-marker profiling, achieving a detection limit of 3×10^4 exosomes using 10 μL of human plasma. However, its sensitivity (10^5 vesicles) and current range (± 7.5 μA) limit its effectiveness for low-concentration exosomes.

Authors in [23] focused on EV markers like CD9, CD63, and CD81, with amperometry achieving a detection limit of 10^8 EVs/mL. Impedimetric analysis using antibody-functionalized gold beads detected CD81 and syntenin EV markers with LOD of 1.9×10^5 particles/mL and 3-5 pM, respectively. Nevertheless, these developed biosensors still fall short in achieving the low LOD required for effective biomarker detection.

To compete with traditional biochemical tests, biosensor platform must achieve minimal LOD, high sensitivity, and excellent selectivity. These performance characteristics are influenced by choice of materials, structural geometries, and biofunctionalization methods used in biosensor fabrication, such as the use of aptamers, proteins, antibodies, nanoparticle coating [24]. Additionally, the design of electronic circuits for potentiostat systems, data acquisition, and signal transmission significantly affects assay performance [25]. A well-designed potentiostat circuit can precisely control electrochemical processes and amplify low current signals from redox reactions, thus enhancing the accuracy and reliability of biochemical tests [26]. Electrochemical biosensors typically operate in one of three primary modes: potentiometric, impedimetric, or voltammetric/amperometric. Potentiometric biosensors detect free ions and are used in protein and pH sensing. For example, the DStat potentiostat [27] measures voltage shifts associated with analyte binding, while a portable, low-power potentiostat developed in another study demonstrated a clear correlation between voltage change and protein concentration in urea samples [28]. On the other hand, impedimetric biosensors measure electrical impedance changes at the electrode-electrolyte interface. Electrochemical impedance spectroscopy (EIS) applies a sinusoidal voltage or current at varying frequencies, identifying target molecules based on variation in amplitude and phase. This technique has been used to detect proteins, enzymes, and other chemical targets [29]. For instance, an EIS-based potentiostat applied 0.2 V sinusoidal voltages across 1 Hz to 10 kHz frequencies to detect neutravidin protein, demonstrating its potential for protein detection [30].

Amperometric biosensors measure current as a function of time or applied voltage. This category includes voltammetry techniques, which involve varying the electrode voltage to monitor current responses, and chronoamperometry (CA), which measures current at a fixed potential [31]. Common voltammetric techniques include SWV, linear sweep voltammetry (LSV), CV, and fast scan cyclic voltammetry (FSCV) [32]. For instance, an amperometric potentiostat demonstrated successful detection of lysozyme at a concentration of 0.5 μg/mL [33]. However, the system exhibited limitations

such as high signal noise, restricted USB connectivity, and the absence of an integrated GUI for real-time data visualization. Moreover, it supported only cyclic voltammetry, limiting its versatility for broader electrochemical sensing applications.

Similarly, the DStat potentiostat [27], an open-source device designed for voltammetric and amperometric measurements, offers customizable functions and compatibility with laboratory-based electrochemical experiments. It is powered via USB and, was tested using potassium hexacyanoferrate (III) and 4-aminophenol solutions, with performance benchmarked against EmStat and Cheapstat platforms. While DStat potentiostat is functional and adaptable, it exhibits several limitations, including increased signal noise issues at low current levels (as low as 600 fA), limited portability due to USB dependence, a narrow voltage range ($\pm$1.5 V), and support only a single current measurement range.

Recent research emphasizes the use of electrochemical potentiostats platforms in detecting cancer-related biomarkers such as circulating tumor DNA, exosomes (including CD63-bearing vesicles), and tumor-associated proteins. For instance, authors in [34] highlighted the potential of multi-target electrochemical biosensors in enabling the characterization of tumor heterogeneity by simultaneously detecting nucleic acids, proteins, and extracellular vesicles, significantly enhancing diagnostic precision for cancer. Similarly, electrochemical ELISA systems have shown potential in detecting common cancer biomarkers like AFP and CEA, with improved sensitivity over optical methods and resilience to solution turbidity interference [35]. The integration of potentiostat-driven biosensors with ML is rapidly transforming diagnostic strategies. A study [36] demonstrated the application of ML algorithms (e.g., artificial neural networks and random forests) to enhance the classification of impedance signals from real-time electrochemical aptamer biosensors, achieving up to 83% accuracy in sample identification related to COVID-19. Additional contributions from [37] described a smartphone-integrated chemiluminescence biosensor system augmented by deep learning models (e.g., ResNet-50) for point-of-care glucose monitoring, demonstrating the versatility of ML across analytes and sensor modalities. Authors in [38] reviewed the role of electrochemical immunosensors in tracking tumor marker dynamics, showing their superiority over traditional histopathology in early-stage detection. Likewise, [39] outlined the promise of nanostructured electrodes (e.g., graphene, metal nanoparticles) in boosting sensitivity and signal-to-noise ratios for detecting ultra-low concentrations of tumor biomarkers. While ML-enhanced biosensors show excellent lab-based performance, integrating them into clinical workflows requires transparent algorithms, large-scale validation, and biosafety evaluation. Efforts such as the ASD-cancer framework for deep-learning-based subtype detection [40] and potentiometric biomarker sensors [41] are key milestones toward these goals. Wang et al. [42] elucidated the role of TIMP-1–CD63 intercellular signaling in pancreatic cancer metastasis and immune escape, showing that CD63 overexpression correlates with poor prognosis in KRAS-mutant tumors. Complementing this, authors in [43] demonstrated a non-faradaic impedance-based potentiostat platform that enables direct quantification of TSG101, another exosomal marker, using electric field-induced lysis, offering an enzyme-free and rapid alternative to traditional ELISA. This approach exemplifies how potentiostats can be adapted for efficient biomarker analysis in serum without compromising protein integrity. Another study [44] reported an aptasensor-integrated microfluidic chip that detects exosomes via electrochemical impedance variations, achieving a low limit of detection of 1.4×10^4 particles/mL and strong discrimination between healthy and cancer patient samples. Similarly, researcher in [45] developed a DNAzyme-walker-based homogeneous potentiostat biosensor that enables HER2+ breast cancer exosome detection with high sensitivity, eliminating complex electrode modifications. Additionally, the lack of standardized protocols for CD63 or TSG101 quantification across biosensor platforms hampers cross-validation, delaying regulatory approval. Finally, while ML algorithms improve classification accuracy, models must be trained on diverse, high-quality datasets to ensure generalizability across patient cohorts.

Numerous studies have focused on developing potentiostat systems tailored for a wide range of applications, including disease diagnosis and drug analysis. These systems vary widely in terms of hardware architecture, voltage ranges, and current measurement capabilities, along with multi-mode electrochemical techniques support. Table 1 provides a comprehensive comparison of recently developed potentiostat platforms, including the proposed system.

Despite advances in potentiostat platforms for electrochemical detection, significant limitations persist. Many platforms, such as the Universal Wireless Electrochemical Detector (UWED) [8], have a narrow current range ($\pm$180 μA), voltage window ($\pm$1.5 V), and high noise levels, resulting in unclear data. The DStat [27] performs well but is costly and relies on USB connectivity, limiting portability. The CheapStat [50] lacks of wireless connectivity and has a restricted voltage range ($\pm$900 mV), limiting its application in wider oxidation reactions. The Enactsense [51] offers promising features but is complex and supports limited electrochemical techniques. SweepStat [52] and KickStat [53] suffer from noise and lack wireless connectivity, the latter also performing poorly in the detection of specific analytes such as cocaine. The MYSTAT [54] has a wide voltage range but slow measurement times and supports only DC measurements. The ABE-Stat [55] improves wireless capabilities but requires noise reduction and calibration. ACEstat [61] provides excellent reproducibility, but is costly and USB dependent. The MiniStat [60] and Portable Laboratory Platform (PLP) [62] perform well but have limited current ranges and lack integrated software. The smartphone-based

TABLE 1. Comparison of related work with the proposed system.

DEVICE	*SUPPORTED TECHNIQUES*	*MICROCONTROLLER*	*COMPLIANCE VOLTAGE*	*CURRENT RANGE*	*DETECTION & CLASSIFICATION METHOD*	*CONNECTIVITY*	*DETECTED SAMPLE*
Sensit Smart [46]	LS,CV,SWV, DP,NP,CA, CC,MA,PAD, OCP,EIS	Commercial	-2V to +2.3V	(±100nA upto ±3mA)	Manual (Experts)	USB	General Application
PalmSense [47]	LS,CV,ACV, SWV,DP, NP,CA,ZRA, CC,MA,	Commercial	±10V	(±100pA up to ±10mA)	Manual (Experts)	Bluetooth,USB	General Application
uStat-I400 [48]	LS,CV,ACV,SWV, DP,NP,CA,ZRA, CC,MA,FAM,PAD, MPAD,LSP,CP,MP, OCP,SCPEIS	Commercial	±4V	(±1nA up to ±10mA)	Manual (Experts)	Bluetooth,USB	General Application
CS100E [49]	LSV,CV,ACV,SWV, DP,NP,CA,ZRA,CC, MA,FAM,PAD, MPAD,LSP,CP, MP,OCP,EIS	Commercial	±12V	(±200pA up to±50mA)	Manual (Experts)	Bluetooth,USB	General Application
DStat [27]	LSV,CV,SWV, DP,CA,CP	ATXmega 256	±1.5V	(±1 uA up to ±100 uA)	Manual (Experts)	USB (Computer)	Hexacyanoferrate Potassium Detection, 4-aminophenol
Cheapstat [50]	LSV,CV,SWV	Atmel XMEGA	±990mV	(±100nA up to±10 uA)	Manual (Experts)	USB (Computer)	Acetaminophen Content in Painkiller, Ascorbic Acid in Orange Juice
Enactsense [51]	LSV,CV,SWV, DP,NP,CA	Arduino Nano 33	±1.5V	±10 uA	Manual (Experts)	Bluetooth (Phone)	Detect DNA Hybridization, Detection of Bacteria
UWED [8]	LSV,CV,SWV, DP,CA,CP	RFduino	±1.5V	±180uA	Manual (Experts)	Bluetooth (Phone)	General Application
SweepStat [52]	CV,LSV,CA	Arduino TEENSY 3.2	±1.5V	±10pA up to ±1.5 uA	Manual (Experts)	USB	Ferrocene methanol Detection
KickStat [53]	CV,CA, NPV,SWV	SAMD21	±0.792V	±1.5nA up to ±10mA	Manual (Experts)	USB	Cocaine Measurement
MYStat [54]	CV,CA, SWV,OCP	PIC16F1459	±12V	±2uA up to ±200mA	Manual (Experts)	USB	General Application
ABE-stat [55]	CV,DPV,EIS	ESP8266 WiFi	±1.5V	±0.1nA up to ±10mA	Manual (Experts)	BLE,Wi-Fi	n.d
PSoC-Stat [56]	CV,SWV,DPV	CY8CKIT-059 PSoC5LP	±2V	±2.5nA up to ±10mA	Manual (Experts)	USB	Lead determination in Water, Glucose Measurements
SStat [57]	CV,LSV,CA	ESP32	±1.5V	(±10nA up to ±0.15mA)	Manual (Experts)	BLE	Lactate Concentration Measurement
Rodeostat [58]	CV,LSV,SV, CV,CA,MSV	Arduino TEENSY 3.2	±10V	(±10nA up to ±1mA)	Manual (Experts)	USB	General Application
EmStat [59]	CV,LSW,DPV, SWV,CA,EIS	Arduino MKR	±3V	1nA to 10mA	Manual (Experts)	USB	General Application
MiniStat [60]	CV,LSW,SWV, CA,ASV	ATXmega 32E5	±1.2V	±10uA	Manual (Experts)	USB	Determination of Copper, Glucose Measurement
ACEstat [61]	CV,LSV,SWV, CA,EIS,CSWV	ARM Cortex M3	±1.1V	50pA to 3mA	Manual (Experts)	USB	Trinitrotoluene (TNT)
Sensor Journal 2019 [62]	CV	Arduino TEENSY 3.2	±1.5V	10nA to 1mA	Manual (Experts)	Bluetooth	Immunodiagnostic of Hepatitis C Virus
NFC Based Potentiostat [63]	CV,CA	CHI 611E	±0.8V	-20uA to +20uA	Manual (Experts)	NFC	Ascorbic Acid Measurement
Wi-Fi Based Potentiostat [64]	DPV, CA, SWV	custom-designed AFE and CC3200 Wifi	±0.4V	n,d	Manual (Experts)	WiFi	General Application
This Work	CV, SWV	Arduino Uno	±2.5V	-2.5mA to +2.5mA -250uA to +250uA -250nA to +250nA	Automatic (Machine Learning)	Bluetooth	CD63 Lung Cancer Biomarkers

Note: (LSV) Linear Sweep Voltammetry, (CV) Cyclic Voltammetry, (SWV) Square Wave Voltammetry, (DPV) Differential Pulse Voltammetry, (NP) Normal Pulse, (CA) Chronoamperometry, (CP) Chronopotentiometry, (ACV) Alternating Current Voltammetry, (PAD) Pulsed Amperometric Detection, (CC) Chronocoulometry, (MA) Multiple Amperometry, (MPAD) Multipulse Amperometric Detection, (LSP) Low Sweep Potential, (MP) Multipotential, (OCP) Open Circuit Potential, (EIS) Electrochemical Impedance Spectroscopy, (FAM) Fast Amperometric Measurement, (ZRA) Zero Resistance Ammeter, (CSWV) Composite Square Wave Voltammetry, (ASV) Anodic Stripping Voltammetry.

system [65] shows potential but needs optimization for sensitivity, specificity, and cost. A significant common gap across all these potentiostat systems is the absence of integrated machine learning, which could enhance data interpretation, automate analysis, and accelerate detection. Addressing these gaps is crucial for the advancement of electrochemical biosensors potentiostat. Therefore, this paper proposes a low-cost, portable machine learning-based potentiostat system with a wide voltage and current range, enhanced sensitivity, wireless connectivity, low noise performance, supporting electrochemical techniques, including CV and SWV, for detection of CD63 lung cancer biomarkers.

The rest of the paper is organized as follows. Section III discusses the methodologies including the system design stages and experimental setup. Section IV discusses the results obtained, and finally Section VI concludes the paper.

III. METHODOLOGY AND EXPERIMENTAL DESIGN

This section describes the technical development of the portable electrochemical potentiostat for EV detection. It details the system architecture, biological sample processing and electrochemical detection methodologies.

A. SYSTEM DESIGN

The proposed system's technical design consists of three main stages: simulation, hardware and software developments. Figure 2 shows a technical overview of the system encompassing both software and hardware components.

1) SIMULATION DESIGN STAGE

The initial stage of system design involves a meticulous simulation process to evaluate the proposed system architecture. This simulation was critical for validating signal generation, circuit integrity, and electrochemical excitation behaviors prior to hardware implementation.

2) HARDWARE DESIGN STAGE

For the hardware stage, the design comprises two aspects, the digital back-end and the analog back-end.

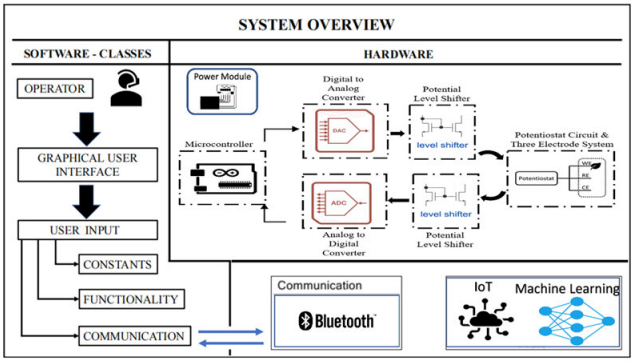

FIGURE 2. Block diagram of the proposed system.

a: THE DIGITAL BACK-END

This aspect focuses on the programming of the microcontroller's firmware which includes configuring the electrochemical techniques characteristics and facilitating seamless communication with the software. Additionally, the Bluetooth module integration and the communication protocol used is specified within the firmware of the microcontroller.

The firmware of the microcontroller is written to enable the generation of the required signals for electrochemical techniques, such as CV, SWV, etc. In addition, the firmware is programmed to read the signal obtained from the developed potentiostat biosensor. The firmware consists of several functions such as CV and SWV representing the electrochemical techniques as well as the associated parameters required including potential range, scan rate, frequency, etc. Subsequently, the Arduino communicates with the Digital-to-Analog Converter (DAC) to generate the corresponding signal. Additionally, the firmware also manages the reading processes of the resulting signal output from the developed potentiostat biosensor, including current, voltage, and impedance, and performs the necessary preprocessing calculation and formatting before transmitting the data to the application software. The microcontroller establishes a communication protocol with the DAC and analog-to-digital converter (ADC) through Inter -Integrated Circuit (I2C) functional. Figure 3 presents the firmware structure and blocks of the microcontroller.

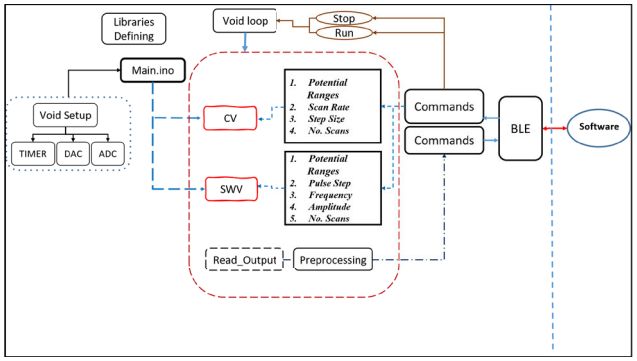

FIGURE 3. Firmware overview of the proposed system.

To ensure portability and wireless operation, the proposed system employs HC-05 Bluetooth module as the connection interface between the hardware and the software components.

Both Wi-Fi and Bluetooth communication protocols were evaluated during the design phase. While Wi-Fi offers greater data range and bandwidth, it significantly increases power consumption, which is not suitable for our portable, battery-powered system. Therefore, HC-05 Bluetooth module is chosen for this work for its low power usage, sufficient data rate for transmitting electrochemical signal values, and stable short-range communication. The use of Bluetooth was further supported by the fact that the electrochemical measurement data is relatively lightweight and does not require high-bandwidth streaming. Additionally, the module integrates easily with the Arduino-based microcontroller and GUI application designed for this system. Although the HC-05 module does not support built-in AES encryption, secure Bluetooth pairing, and application-layer protection mechanisms, were implemented. These include secure user authentication and role-based access control (RBAC) to prevent unauthorized access, input validation to mitigate injection and manipulation risks, and encryption of sensitive data using platform-level APIs. These security measures collectively enhance the reliability and robustness of the system for clinical and portable use.

b: THE ANALOG BACK-END

The analog back-end design comprises power modules circuit, voltage level shifters circuits, calibration unit, potentiostat circuits, as well as analog and digital converters.

Analog and digital circuit components have different requirements of power level ranging from +5V to -5V. Therefore, a positive and negative supply regulators are used to satisfy the requirements. UA78L05 step down linear regulators is used to provide a fixed +5V output required to power up the positive rail of operational amplifiers (Op-Amp), Arduino, Bluetooth, ADC and DAC components. Similarly, ICL7660 which is a monolithic CMOS negative power regulator is used to deliver a -5V output required for the negative rail of the operational amplifiers.

The output voltage generated by the DAC circuit is unipolar (positive range) and needs to be converted to a bipolar (positive and negative) voltage to support electrochemical experiments particularly when a negative potential is required for specific chemical reactions. To achieve this, the system incorporates an operational amplifier-based level shifter circuit that converts the unipolar DAC output into a bipolar voltage signal. This circuit consists of two operational amplifiers: Op-Amp A, which performs the level shifting, and Op-Amp B, which functions as an inverting amplifier. In addition, a reverse level shifter circuit is implemented to convert the bipolar signal back to a unipolar form ranging from 0-5 V, making it compatible with the ADC and the microcontroller. Voltage level offsets required for both

shifting circuits are adjusted using a calibration unit, which consists of two precision potentiometers.

A potentiostat circuit is essential for electrochemical experiments, controls voltage and measures current between electrodes. The core components of a potentiostat are primarily based on various arrangements of operational amplifiers using LMC6484. Op-Amp buffer circuit, voltage follower circuit and transimpedance amplifier (TIA) are employed to construct the developed potentiostat circuitry. In order to prevent loading of the earlier Op-Amp stages by the current drawn from the electrochemical cell, a buffer circuit with smoothing capacitor in the feedback loop, is inserted between the counter electrode and the level shifter voltage circuit output. A voltage follower is employed to maintain a constant potential at the reference electrode while minimizing current draw. A transimpedance circuit is also employed to convert the current of the electrochemical cell, specifically working electrode, into the corresponding voltage to be measured.

The use of the DAC in the proposed system is to generate the suitable analog signal for the electrochemical techniques with high precision and accuracy. The microcontroller used in the system does not provide a DAC circuit integrated with it and the digital output pins of the Arduino is not capable of generating a precise analog output. Therefore, MCP4725, which is a single channel, 12-bit, DAC converter with integrated electrically erasable programmable read-only memory (EEPROM) and an I2C compatible serial interface, is utilized in the design. ADC used here is ADS1115, which is an ultra-small, low-power, 16-bit precision ADC with an internal reference voltage. The ADS1115 is designed to draw only about 150 μA in continuous mode. Additionally, the ADS1115 uses the I2C communication protocol, similar to the protocol used by DAC, resulting in less error and low latency. Figure 4 presents the schematic diagram of the proposed system while figure 5 illustrates the experimental setup for the developed system.

The power consumption of the developed wireless electrochemical biosensor system was evaluated to assess its suitability for portable and field-based applications. Current draw was measured under various operational states as follows: Idle mode (with no Bluetooth activity), the system consumed approximately 60–65 mA. During active mode, which includes electrochemical measurement and Bluetooth transmission, the system utilized approximately 80–90 mA. The peak current draw, typically observed during Bluetooth pairing or intensive analog read/write operations, reached up to 100 mA. Table 2 shows the estimated current drawing for each components of the developed system.

To estimate the operational time, a standard 9V alkaline Energizer battery (nominal capacity: 600 mAh under light loads) was used as the power source. Under continuous operation, assuming an average current draw of approximately 80 mA during continuous measurements and wireless data

TABLE 2. Power consumption of developed system.

Component	Typical Operating Voltage	Average Current Consumption
Arduino Uno	5 V	$\sim$ 45–50 mA
LMC6484 x2	$\pm$5 V	$\sim$ 2.2 mA
MCP4725 (DAC)	3.3–5 V	$\sim$ 0.25–0.5 mA
ADS1115 (ADC)	5 V	$\sim$ 0.15–0.3 mA
Bluetooth (HC-05)	5 V	$\sim$ 30–50 mA (active) $\sim$ 8 mA (idle)
UA78L05	9 V $\rightarrow$ 5 V	$\sim$ 5–10 mA
ICL7660	+5V $\rightarrow$ -5V	$\sim$ 0.5–1 mA
Resistors and Capacitors	N/A	Negligible (< 1 mA in total)

transmission, the estimated battery life is given by:

$$\text{Battery Life} = \frac{600\,\text{mAh}}{80\,\text{mA}} \approx 7.5\,\text{hours} \tag{1}$$

On the other hand, under an intermittent operation, whereby measurements are taken every 10 minutes (600 seconds), with each measurement and transmission event lasting 20 seconds at 90 mA, and the system remains in a low-power sleep mode of approximately 15 mA for the remaining 580 seconds, the average current consumption can be estimated as:

$$\text{Average Current} = \frac{(90 \times 20) + (15 \times 580)}{600} \approx 17.5\,\text{mA} \tag{2}$$

This yield a battery life of:

$$\text{Estimated Battery Life} = \frac{600\,\text{mAh}}{17.50\,\text{mAh}} \approx 34.3\,\text{hours} \tag{3}$$

These estimates demonstrate that the system can support extended usage under optimized measurement intervals, highlighting its potential for portable and semi-continuous point-of-care diagnostic applications.

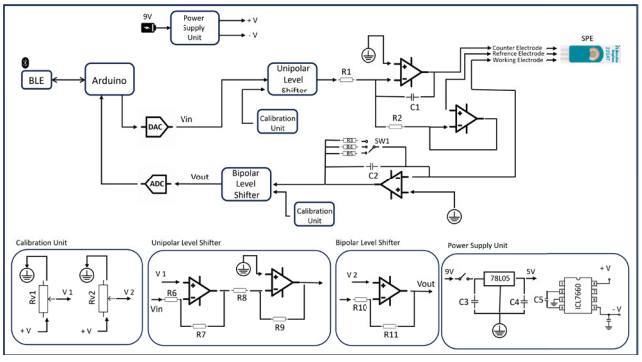

FIGURE 4. Hardware schematic diagram.

The cover and enclosure for the developed portable device is printed using 3D printer. The material selected for 3D printing is ABS, known for its durability and high-temperature tolerance. These properties enhance the robustness of the cover while supporting a compact and

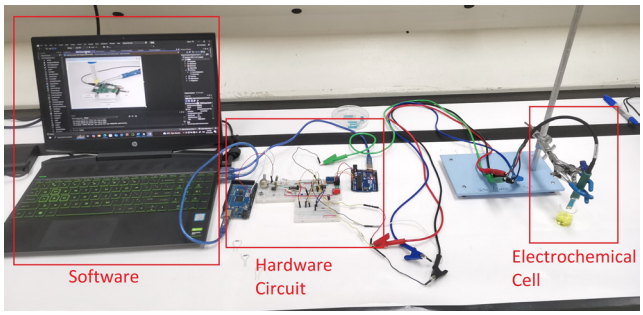

FIGURE 5. Experimental setup.

portable design. This entire platform measures 15cm x 10cm x 5cm, contributing to a more user-friendly design. Figure 6 shows the prototype of the developed potentiostat platform.

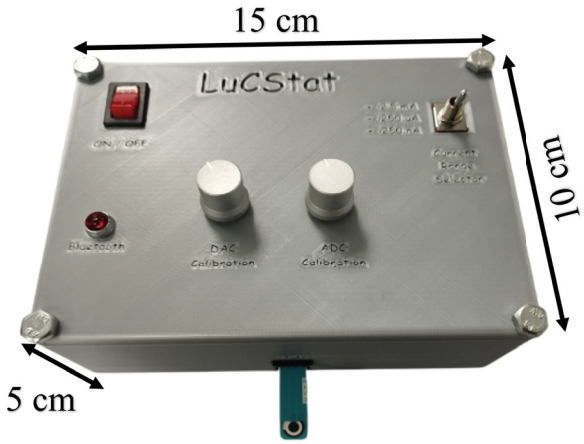

FIGURE 6. Developed system's prototype.

3) SOFTWARE APPLICATION DESIGN STAGE

The design stage of the software and application comprise of designing the interface layout with user input parameters, data visualization and finally the integration of IoT and machine learning model.

a: USER INPUT

A GUI is designed based on Windows Form, which serves as an interactive platform for the users to input the necessary parameters to control the electrochemical techniques. As shown in Figure 7, the user input categories include ''Constants'', which represent the electrochemical measurement parameters. ''Functionality'', which defines the type of electrochemical technique being performed and ''Communication'' which handles the communication protocol and ports selection.

b: REAL TIME DATA VISUALIZATION

The results obtained from the system are visualized through graphical plots that display the relationship between the applied potential and the corresponding electrochemical

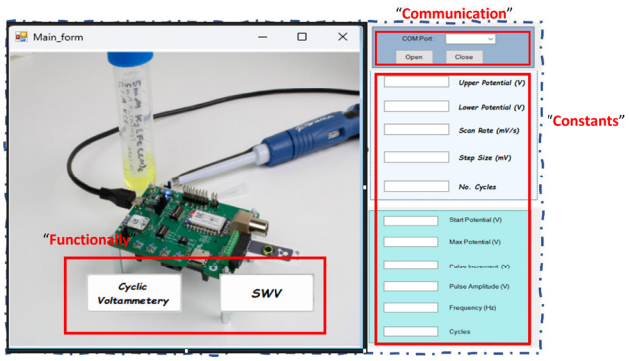

FIGURE 7. User input parameters.

current response. These plots are tailored to the specific electrochemical techniques performed, such as CV or SWV, facilitating a precise representative of the experimental data. Real-time plotting allows users to dynamically monitor electrochemical responses, track signal trends, and extract key analytical parameters efficiently. The graphical output is continuously updated as new data is transmitted from the hardware, thereby supporting real-time data acquisition and visualization.

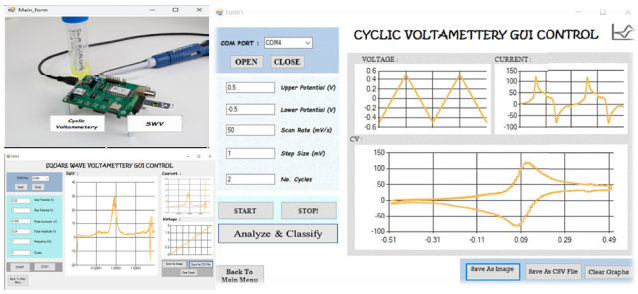

FIGURE 8. Real time platform's data visualization.

c: IoT AND MACHINE LEARNING

The developed potentiostat biosensor platform enables the transmission of the resulting electrochemical outcome to cloud platforms. This facilitates instant data access, further data analysis, and remote monitoring. In the proposed system, Firebase database service is utilized as a cloud storage solution for the experiment's outcomes ensuring data is securely stored and easily accessible. Additionally, by maintaining active connections on the Personal Computer (PC), the system can automatically upload the data to cloud services and allow authorized users to access the data and perform further analysis. The Firebase was selected as it offers straightforward and reliable integration with the software environment, which simplifies the development and maintenance of the GUI application. At the application level, user authentication and encryption protocols ensure that only verified data is transmitted and received. Firebase offers several key features that enhance data security and transmission

stability including, encrypted HTTPS communication, which ensure that all data uploaded from the client application to Firebase is securely transmitted. It also provides user-based access control rules, enabling the system to restrict access to only authorized users and devices. Besides that, it supports automatic data syncing and offline caching, which ensures that data is reliably queued and uploaded even when connectivity is briefly interrupted.

The proposed system also employs machine learning algorithms to enhance data interpretation by identifying patterns and performing classification on data obtained from various applied electrochemical techniques. This integration is achieved through the use of widely machine learning libraries, such as TensorFlow, PyTorch, and Keras, which facilitate the development of the machine learning model. A Windows Forms application serves as the GUI, enabling users to interact with the machine learning model seamlessly. Among the algorithms employed, the Random Forest classifier, is a machine learning algorithm that falls under the category of ensemble learning. It is a commonly used machine learning algorithm that combines the output of multiple decision trees to reach a single result, thereby improving overall accuracy and robustness. Random Forests is robust to noise, handle small datasets well, and provide feature importance, making them highly interpretable. In the proposed system, Random Forest classifier is chosen for its ability to handle complex interactions between features and its robustness against overfitting, ensures reliable classification of electrochemical outcomes.

The machine learning model was trained and evaluated using a dataset consisting of 75 electrochemical measurements obtained from the proposed biosensor system as well as from a commercial potentiostat, under identical conditions, utilizing both CV and SWV techniques. Each measurement corresponds to either a positive sample (indicating the presence of CD63 protein lung cancer biomarkers) or a negative sample (indicating the absence of biomarkers). For each electrochemical measurement, a set of critical features was extracted to serve as the input vector for the machine learning models. These features include the minimum, maximum, standard deviation, and median values of both the voltage and the corresponding current responses. Additionally, parameters specific to the electrochemical techniques such as the scan rate for CV, while for SWV, the step potential, pulse amplitude, and frequency were also incorporated as input features. For CV, the maximum current values observed during the forward and reverse scans were extracted, while for SWV, the peak current and the corresponding peak potential were identified and used as features. Furthermore, the area under the curve (AUC), representing the integrated voltammetric response and indicating the total charge transferred during the electrochemical reaction, was also included as a feature in the machine learning model. These electrochemical parameters were chosen as features due to their direct correlation with the concentration and redox behavior of the CD63 protein. All current and voltage-related features were normalized to a consistent scale to account for variability in sensor surface area and hardware tolerances. It is worth nothing that the dataset was moderately imbalanced, with 43 positive samples and 32 negative samples. To address this imbalance and prevent classifier bias toward the majority class, we applied the Synthetic Minority Over-sampling Technique (SMOTE) during the training phase. This ensures a more balanced representation of classes, thereby enhancing the model's ability to accurately classify both positive and negative cases.

To ensure the reliability and reproducibility of results, meticulous care was taken in acquiring and preprocessing the electrochemical data used in this study. The dataset originated from experimental measurements using the developed wireless electrochemical biosensor potentiostat system was obtained from exosome samples isolated from A549 lung cancer cell lines. The exosome isolation was performed using sucrose cushion ultracentrifugation, followed by aptamer-based immobilization on the working electrode targeting the CD63 protein biomarker. Electrochemical measurements were performed using CV and SWV techniques on a screen-printed gold electrode (SPGE) functionalized with a 5-thiolated CD63 aptamer. For each concentration of exosome sample, a minimum of three independent measurements were conducted to ensure statistical consistency. The electrochemical parameters were configured as shown in Table 3. All experiments were conducted under controlled laboratory conditions to mitigate the influence of external factors such as temperature and humidity. Prior to the main measurements, the potentiostat system was calibrated using standard redox probes, such as 5 mM potassium ferricyanide in phosphate-buffered saline (PBS), to ensure consistent performance. Real-time signal monitoring was used to identify and eliminate any datasets affected by transient noise. Measurements exhibiting significant noise spikes or abnormal baselines were discarded and re-recorded. Raw electrochemical data, consisting of current-voltage profiles, were subjected to several preprocessing steps before machine learning analysis. These preprocessing steps to ensure that the electrochemical signals were consistent, interpretable, and suitable for feature extraction, enabling robust pattern recognition and classification by the machine learning algorithms integrated into the platform.

TABLE 3. Comparison of CV and SWV parameters.

CV		SWV	
Parameter	**Value**	**Parameter**	**Value**
Potential Range	[-0.5 to 0.5] V	Potential Range	[-1 to 1] V
Scan Rate	50 mV/s	Pulse Amplitude	25 mV
Step Size	2 mV	Frequency	15 Hz
Cycles No	3	Pulse Increment	4 mV

The working concept of the machine learning integration into the software application is shown in Figure 9. Once the user performs the chosen electrochemical techniques, the resulting outcomes obtained in terms of current and

voltage values as well as other parameters are saved. Then, preprocessing stage involves filtering and feature extraction of the results, to be fed into the machine learning model. Finally, the machine learning model analyze and classify the experimental outcome into a suitable class, specifically lung cancer or non-cancer case based on the presence or absence of the CD63 biomarker in the sample.

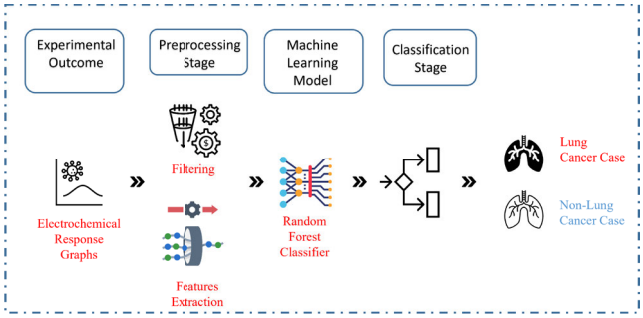

FIGURE 9. Machine learning detection flow.

The developed portable electrochemical potentiostat was applied for EV exosomes detection using the following biological and electrochemical methodologies.

B. BIOLOGICAL SAMPLE PROCESSING

1) CELL CULTURE AND EV ISOLATION

A549 cells were cultured in DMEM (Thermo Scientific), supplemented with 10% fetal bovine serum (FBS, Thermo Scientific) and 1% penicillin/streptomycin (Sangon Bio), in a humidified incubator at 37°C with 5% CO_2. EVs released from cultivated A549 cells were collected following procedures described by [66] and [67]. When cells reached approximately 80% confluency, the culture medium was replaced with serum-free DMEM and incubated for 48 hours. The conditioned medium was collected and sequentially centrifuged to remove cellular debris: 500×g for 5 min, followed by 2,000×g for 15 min, and 10,000×g for 30 min (Thermo Scientific Sorvall). The resulting supernatant was transferred to an ultracentrifuge tube (Beckman 344058) and a 30% (w/w) sucrose solution prepared in Milli-Q water was carefully layered at the bottom using a Pasteur pipette. Ultracentrifugation was performed using a swinging-bucket rotor (SW28, Beckman Coulter Optima L-90K) at 100,000×g for 1.5 hours at 4°C. Subsequently, 3 mL of the sucrose layer was aspirated from the bottom, mixed with 1×PBS and transferred into a polycarbonate centrifuge bottle (Beckman 355618). A second ultracentrifugation step was performed using a fixed-angle rotor (Type 70 Ti) at 100,000×g for 1.5 hours at 4°C. The final EV pellet was resuspended in 1×PBS.

2) EV CHARACTERIZATION AND VALIDATION

The size distribution and mean particle number of the isolated EVs were determined using nanoparticle tracking analysis (NTA) (NanoSight NS300, Malvern Panalytical). NTA confirmed that the vesicles isolated from A549 cell culture supernatant predominantly fell within the 50–150 nm size range, with a peak around 100 nm. These particles are commonly associated with exosomes based on their characteristic size distribution. Expression of the EV surface marker CD63 was confirmed by immunoblotting as shown in Figure 10. The sample is referred as EVs throughout the manuscript in accordance with MISEV 2018 guidelines [68]. Briefly, the total protein concentration of the EV sample was quantified using the bicinchoninic acid assay, following the manufacturer's protocol (Micro BCA™Protein Assay Kit, Thermo Fisher Scientific). An aliquot of the isolated EV sample containing 638 ng of total protein was spotted onto a nitrocellulose membrane and blocked with 1% (w/v) BSA in PBS-T (1× PBS with 0.05% (v/v) Tween-20) for 1 hour at room temperature. The membrane was then incubated with 5 mL of anti-human CD63 primary antibody (Ultra-LEAF™Purified anti-human CD63 Antibody, BioLegend), diluted 1:1000 in the blocking buffer and incubated for 16 hours at 4°C. After five washes with PBS-T, the membrane was incubated with HRP-conjugated secondary antibody (HRP Goat anti-mouse IgG, BioLegend), diluted 1:2500 in blocking buffer, for 1 hour at room temperature. The washing step was repeated. The signal was developed using WesternBright ECL HRP substrate (Advansta Inc.) and visualized using a gel documentation system.

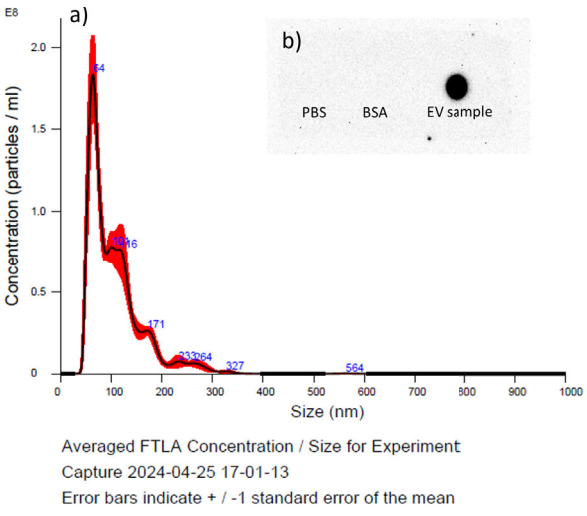

FIGURE 10. (a) Size distribution of EVs isolated from A549 cell culture supernatant, as determined by nanoparticle tracking analysis (NTA) using the NanoSight NS300 system, (b) Presence of CD63 protein marker on the surface of isolated EVs was validated by dot blot assay. 1x PBS and bovine serum albumin (BSA) protein were used as controls.

C. ELECTROCHEMICAL DETECTION METHODOLOGY

1) ELECTRODE PREPARATION AND MODIFICATION

Screen-printed gold electrodes (Au-SPE, Metrohm) were prepared according to previously reported protocols [69], [70]. Briefly, electrodes were cleaned with a 1:1 (v/v) ethanol–Milli-Q water solution, rinsed thoroughly with Milli-Q water

and dried under a stream of nitrogen gas. Electrochemical cleaning was carried out by CV technique (Metrohm DropSens) in 0.1 M H_2SO_4, scanning from -0.3V to +1.7V for 10 cycles (step potential: 0.002V, scan rate: 0.3V/s). The process was repeated in 0.5 M H_2SO_4. After cleaning, 5 μL of washing buffer (20 mM sodium phosphate buffer containing 0.15 M NaCl, pH 7.4) was applied to the working electrode for 10 min, followed by Milli-Q rinse and drying. A standard desalted thiolated CD63 aptamer (5)-/5ThioMC6-D/CACCCCACCTCGCTCCCGTGACACTAATGCTA-3) was obtained from Integrated DNA Technologies [71]. The 100 μM stock solution was reduced with DTT to cleave disulfide bonds and diluted to 4 μM in incubation buffer. The working electrode was incubated with 5 μL of the reduced aptamer solution at 4°C for 2 hours. After incubation, the electrode was rinsed thoroughly with washing buffer and dried. To minimize nonspecific adsorption, 5 μL of 6-mercapto-1-hexanol (MCH) in 1×PBS was applied to the working electrode and incubated at 4°C for 1 hour. The electrode was rinsed again with washing buffer and dried.

2) DETECTION PROTOCOL AND MEASUREMENT PARAMETERS

To perform EV detection, 10 μL of EV sample (in 1×PBS) was applied to the aptamer-modified Au-SPE and incubated for 30 min. The electrode was then gently rinsed with 3 mL of washing buffer. CV and SWV measurements were performed using 100 μL of 5 mM potassium ferricyanide $K_3[Fe(CN)_6]$ in 1×PBS as the redox probe using parameters in Table 3. For the negative control, the aptamer-modified Au-SPE was incubated with 1× PBS instead of EVs.

IV. RESULT AND DISCUSSION

In this study, the tetraspanin protein CD63, a well-established surface marker of EVs was employed as the target biomarker. The presence of CD63-positive EVs are often elevated in lung cancer patients, and are closely associated with disease progression and metastasis. The performance of the proposed potentiostate system was evaluated using two widely used electrochemical techniques, namely, CV and SWV.

The electrochemical detection mechanism of the proposed biosensor system leverages on the highly specific biorecognition event that occurs at the sensor's surface. Upon modification, the CD63-specific aptamer forms a stable and selective recognition layer on the sensor's working electrode. When EVs containing CD63 protein on their membrane are introduced to the electrode, the surface-anchored aptamer molecules recognize the protein and bind to it via high affinity, non-covalent interactions forming a stable complex. This binding event and the presence of large, negatively charged EVs on the electrode's surface alters its interface as there is an increase in steric hindrance and a change surface charge density. The surface-bound EVs impedes the access of the redox mediator, $[Fe(CN)_6]3$ to the electrode surface leading to a decrease in electron transfer and subsequently a decrease in current which is measurable through voltammetry. The electrochemical response directly correlates with the presence and abundance of EVs enabling quantitative detection.

A. CYCLIC VOLTAMMETRY (CV)

Cyclic Voltammetry is a fundamental electrochemical technique used to characterize redox reactions and examine the behavior of electroactive species in a given sample. Figure 11 illustrates the CV responses of samples with and without CD63 biomarker. As depicted in Figure 11, samples containing CD63 exhibit a noticeably higher peak current compared to the control samples (without biomarker) indicating enhanced electrochemical activity in the presence of the biomarker. The presence of the biomarker causes a slight shift in the peak potential is also observed, suggesting alterations in the kinetics of the redox process or changes in the electroactive properties induced by the presence of CD63-positive EV.

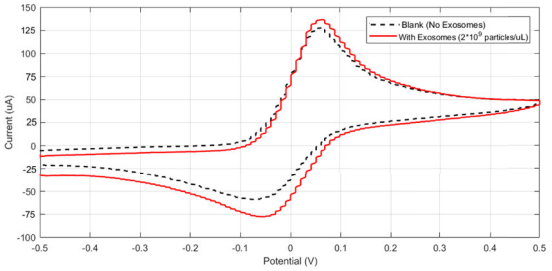

FIGURE 11. Cyclic voltammetry with and without EVs at scan rate of 50 mV/s.

The accumulation of EVs on the electrode surface, changes its electrochemical characteristics, thereby improving electron transfer reactions. CV measures both capacitive and faradaic currents, making it less effective than SWV at suppressing capacitive contributions. As a result, SWV is generally more suitable for detecting small faradaic signals arising from redox reactions. In this study, a high concentration of EVs 2×10^9 particles/mL was utilized, which may have led to significant accumulation of negatively charged EVs on the electrode surface. This accumulation likely has altered the electric double layer and enhanced electron transfer, contributing to an increased peak current compared to the control sample without EVs. The observed slight differences in CV responses between samples with and without EVs demonstrates the potential of this method for detecting CD63, a protein lung cancer biomarker. However, the peak current separation was less distinct than that observed with the SWV techniques. While CV offers advantages such as simplicity and rapid experiment time, it lacks sensitivity at lower sample concentrations. Overall, the CV responses confirm the operational capability of the developed potentiostat platform for the detection of lung cancer biomarkers.

B. SQUARE WAVE VOLTAMMETRY

Figure 12 presents the SWV responses of the developed system for two different samples, with and without EVs. Gold electrodes, used in this work, are widely chosen for electrochemical biosensors because of a combination of chemical, electrical, and surface properties that make them ideal for sensitive and specific detection. Specifically, gold is a highly conductive metal, allowing efficient electron transfer between the electrode and redox probe. This leads to sharp, well-defined current peaks and better signal-to-noise ratios.

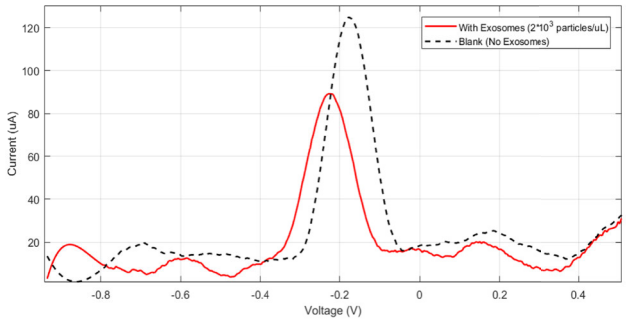

FIGURE 12. Square wave voltammetry with and without EVs at frequency of 15 Hz.

Figure 12 shows that the measured peak current is lower in the presence of EVs. Moreover, the redox peak is slightly broader and a shift in peak potential is observed in the presence of EVs.

When EVs bind to the electrode surface, they alter the local electrochemical environment. The binding of EVs changes the density of the redox mediator at the electrode surface. The decreasing peak current observed in SWV for samples containing EVs, compared to sample without EVs, reveals a complex interplay of electrochemical processes and surface interactions. In SWV, the peak current is highly sensitive to the changes on the electrode surface and the surrounding electrochemical environment. As EVs adhere to the electrode, they block active sites, form insulating layers, and alter the properties of the electrical double layer at the electrode interface, all of which reduce the effective surface area for electron transfer and decrease the current response.

Zeta potential measurement indicates EVs have a negative surface charge [72]. The negatively charged EVs repels the $[Fe(CN)_6]3$ anion, hindering access of the redox probe to the electrode surface. This suppresses electron transfer, resulting in a decreased peak current in the presence of EVs. EVs with strong zeta potential can also alter the local electric double layer at the electrode interface. This affects the capacitive current and can shift and broaden the redox peaks, indirectly influencing the measured peak current.

In blank samples, the absence of specific EVs might lead to an increased in non-specific adsorption of other species (e.g., impurities, ions) that contribute to a higher capacitive current, appearing as a peak in SWV. Additionally, in the absence of EVs, the rate of electron transfer is higher and the electric double layer is characteristic of the redox probe, resulting in a higher peak current and narrower redox peak.

To validate the results obtained from the developed potentiostat platform, a comparative analysis was conducted using the uStat8000 by DropSens, a top-notch commercial lab-based potentiostat. The same samples were analyzed using both the developed biosensor and the uStat8000 under identical conditions. Figure 13 illustrates a comparison of results obtained for the proposed electrochemical biosensor platform and the commercial uStat8000 for two electrochemical techniques, CV and SWV. The graphs provide insight into the current responses of both systems.

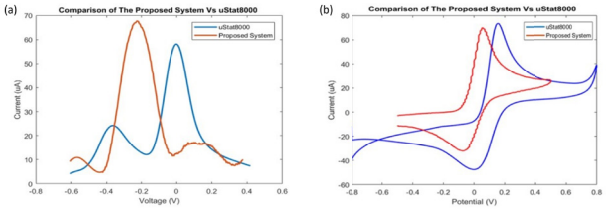

FIGURE 13. Performance comparison of the proposed electrochemical biosensor platform with uStat8000, (a) SWV response and (b) CV response.

C. SENSITIVITY PERFORMANCE

Sensitivity is a critical performance metric that quantifies the device's ability to detect changes in the concentration of analytes, such as biomarkers. It is defined as the change in the output signal (current) per unit change in analyte concentration, measured in μA per particles/mL. High sensitivity is paramount in applications requiring precise quantification of low-abundance species, such as in early cancer detection, where biomarkers may be present in extremely low concentrations. This is because a potentiostat with high sensitivity can detect minute variations in analyte levels. This metric is not only crucial for identifying the presence of target molecules but also for ensuring accurate and reliable measurements across a range of concentrations. Sensitivity directly impacts the LOD of the potentiostat, which is the key parameter in evaluating its overall performance. Figure 14 shows the system's sensitivity responses for various concentration of CD63 protein lung cancer biomarkers. As for the developed potentiostat system, sensitivity is related to the change in current μA per log unit change in concentration particles/mL. The concentration values are converted to their corresponding logarithmic form to account for the wide range of concentrations. Table 4 presents the relationship between EV concentration and the corresponding peak current response for the developed electrochemical biosensor platform. A clear trend is observed where the peak current increases with higher EV concentrations.

This relationship is also evident in the logarithmic values of the concentrations. This indicates that the developed platform is capable of detecting varying levels of EV concentration, demonstrating its sensitivity and effectiveness

TABLE 4. Exosomes concentration and peak current response for the developed system.

Concentration (particles/mL)	$\log_{10}$(Concentration), x	Peak Current (μA), y
2×10^1	1.3010	62.5
2×10^2	2.3010	69.04
2×10^3	3.3010	82.17
2×10^4	4.3010	89.12
2×10^5	5.3010	91.32
2×10^7	7.3010	102.4

in electrochemical biosensing for CD63 protein lung cancer biomarker detection.

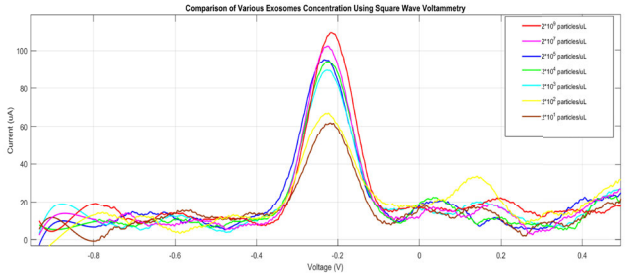

FIGURE 14. Comparison of various SWV responses for various samples concentration.

Sensitivity is defined as:

$$\text{Sensitivity} = \frac{\text{Cov}(x, y)}{\text{Var}(x)} \tag{4}$$

where,

$$\text{Cov}(x, y) = \frac{(x - \bar{x})(y - \bar{y})}{n} \tag{5}$$

$$\text{Var}(x) = \frac{(x - \bar{x})^2}{n} \tag{6}$$

where n is the number of observations, $\bar{x}$ is the mean value of concentration in logarithmic form, and $\bar{y}$ is the mean value of peak currents.

From Table 4, $\bar{x}$ and $\bar{y}$ can be expressed as:

$$\bar{x} = \frac{\sum x}{n} = \frac{1.3 + 2.3 + .. + 7.3}{7} = 4.729 \tag{7}$$

$$\bar{y} = \frac{\sum y}{n} = \frac{62.5 + 69.04 + \ldots}{7} = 86.35 \tag{8}$$

Therefore, from Eq (7) and Eq (8), covariance and variance can be determined as:

$$\text{Cov}(x, y) = \frac{(1.3010 - 4.729)(62.5 - 86.35) + \ldots}{7} = 40.251 \tag{9}$$

$$\text{Var}(x) = \frac{(1.3010 - 4.729)^2 + \ldots}{7} = 7.757 \tag{10}$$

Substituting Eq (9) and Eq (10) into Eq (4), sensitivity can be written as:

$$\text{Sensitivity} = \frac{\text{Cov}(x, y)}{\text{Var}(x)} = 5.188 \tag{11}$$

Thus, from Eq (11), the sensitivity of the developed potentiostat is approximately 5.188 μA per log unit of concentration (particles/mL). This higher sensitivity value indicates that the developed potentiostat is more responsive to changes in concentration to detect variations in EV concentrations, demonstrating the effectiveness of the proposed method.

To evaluate the quantitative capability of the developed biosensor for CD63 protein detection, a calibration curve was constructed by plotting the peak current response (in μA) against the logarithmic concentration of CD63. Six concentrations ranging from 2×10^1 particles/mL to 2×10^7 particles/mL were tested using the SWV technique as shown in Table 4. A linear regression analysis revealed a strong correlation between the peak current and log10(concentration). Linear fit expression can be written as:

$$\bar{y} = mx + b \tag{12}$$

where, m refers to the sensitivity and b is y-intercept. Eq (12) can be written as:

$$\bar{y} = 5.188 \cdot x + 56.16 \tag{13}$$

R^2 is defined as:

$$R^2 = 1 - \frac{SS_{\text{res}}}{SS_{\text{tot}}} \tag{14}$$

where, SS_{res} refer to the sum of squares of Residuals, while SS_{tot} refer to the sum of squares. Both can be determined as:

$$\text{SS}_{\text{tot}} = \sum (y_i - \bar{y})^2 = 1297.9 \tag{15}$$

$$\text{SS}_{\text{res}} = \sum (y_i - \hat{y})^2 = 38.70 \tag{16}$$

The regression showed a correlation coefficient $R^2 = 0.97$, indicating an excellent linear relationship over the tested range. Figure 15 shows the R^2 curve, which illustrates the goodness of fit of the developed system. The sensitivity of the biosensor, defined as the slope of the calibration curve, was found to be 5.188 μA per log unit concentration, which demonstrates the device's high responsiveness to changes in CD63 levels. This linear dynamic range (LDR) spans from 2×10^1 particles/mL to 2×10^7 particles/mL, which covers a clinically relevant concentration range for exosome-based biomarker detection, demonstrates the system's capability for quantitative detection of CD63 within a clinically relevant range.

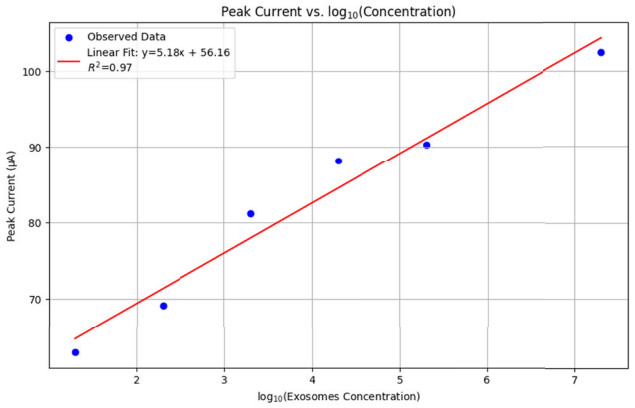

FIGURE 15. Linear regression curve with R^2 value of the biosensor's response to varying CD63 concentrations.

D. CLASSIFICATION USING MACHINE LEARNING MODELS

A machine learning model, specifically Random Forest Classifier was developed for automated interpretation of the electrochemical data obtained from the proposed system. In addition to the Random Forest model, other well-established supervised learning algorithms were also developed and evaluated for comparative performance analysis. These include the Support Vector Machine (SVM), Decision Tree, and K-Nearest Neighbors (KNN) classifiers. Each model was trained using the same dataset and subjected to identical preprocessing steps to ensure a fair comparison. This comparative analysis helped determine the most suitable algorithm for reliable and real-time classification of lung cancer biomarkers from electrochemical signals. Among the tested models, the Random Forest classifier demonstrated superior overall performance, especially in balancing sensitivity and precision, making it the most appropriate choice for integration into the final system for real-time biomarker detection. The models were trained using a dataset of voltammetric responses, which corresponds to known concentrations of CD63 protein lung cancer biomarkers (positive samples) as well as responses from samples without the CD63 protein lung cancer biomarkers (negative samples) taken from 75 experiments's observations. The training process involved feature extraction and feature selection.

To ensure the reliability and generalization of the developed model, rigorous statistical validation techniques were implemented, including k-fold cross-validation and bootstrapping. The dataset was initially split into 70% for training and 30% for testing. The performance metrics presented in Table 5 such as accuracy, precision, recall, and F1-score, were derived solely from the testing dataset, which was not seen during training. Additionally, a 5-fold cross-validation technique was employed during the model training phase to further assess the model's consistency and prevent overfitting. In this process, the training data was divided into five equal subsets, with the model iteratively trained on four subsets and validated on the fifth. This cycle was repeated five times, and the results were averaged to evaluate the model's stability across different data partitions. The combination of cross-validation and independent test evaluation provides strong evidence of the model's ability to generalize well to unseen experimental data. Although all data were obtained under controlled lab conditions, the use of machine learning validation techniques offers a reasonable estimate of the model's potential performance. In parallel, the bootstrapping technique involved the resampling of the original dataset with replacement to generate multiple pseudo-replicates. These replicates enable estimation of the variability and distribution of model performance metrics, thereby reinforcing the robustness and statistical confidence of the findings. The integration of these methodologies not only strengthens the credibility of the machine learning's models outcomes, but also enhances the model's reliability when applied to real-world biosensor data for lung cancer detection, specifically, CD63 protein biomarkers.

TABLE 5. Performance metrics of different machine learning models for CV and SWV cases.

Metric	Random Forest		SVM		KNN	
	CV	SWV	CV	SWV	CV	SWV
Accuracy	83.5%	87.5%	70.0%	62.5%	80.0%	75.0%
Precision	100.0%	86.4%	100.0%	62.0%	100.0%	80.0%
Recall	67.0%	89.0%	50.0%	100.0%	67.0%	80.0%
F1-Score	80.24%	87.6%	67.0%	77.0%	80.0%	80.0%

Key metrics such as accuracy, precision, recall, and F1-score were calculated to assess the model's effectiveness in predicting biomarker detection. Table 5 summarizes the performance metrics of the machine learning model. From Table 5, it can be seen that the developed model, specifically the Random Forest Classifier for CV data, achieved an accuracy of 83.5%, which reflects a relatively high overall performance. The random forest model for CV achieved a precision of 100%, indicating that the model has no false positives and is very reliable in predicting positive outcomes. However, recall is 67%, which means that the model only identified 67% of the actual positive cases. The F1-score of 80.24% balances the high precision and moderate recall, indicating that while the model is very accurate in its positive predictions.

In contrast, the SWV case demonstrated an improved performance with an accuracy of 87.5%, and a consistent precision and recall of 86.4% and 89%, respectively, resulting in a balanced and strong F1-score of 87.6%. This indicates that the random forest model for the case of SWV, not only correctly identifies the majority of positive cases but does so with high reliability. Confusion matrix assessment tool is used to assess the performance of a system, where it provides a precise representation of the model's classification performance by accurately displaying the outcomes for both true and false classes. Figure 16 and 17 present the confusion matrix of the Random Forest for the two developed models based on CV and SWV obtained data, respectively.

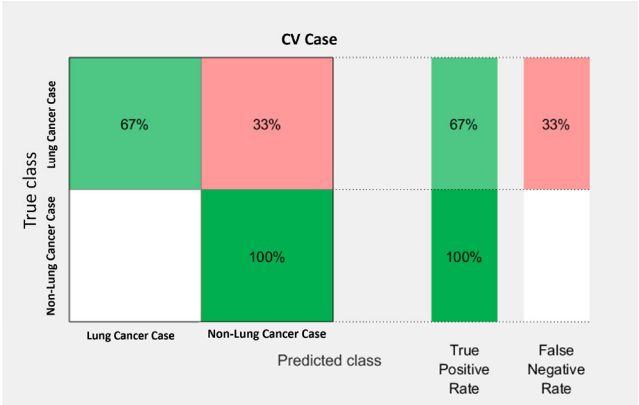

FIGURE 16. CV case confusion matrix of the random forest classifier model.

FIGURE 17. SWV case confusion matrix of the random forest classifier model.

The confusion matrices in Figure 16 and 17 revealed several notable insights into the misclassifications trends for each model. For the Random Forest classifier, which achieved the highest performance among all models, false negatives were the most common misclassifications type. In particular in the CV data where Recall is 67%. This indicates that some cancer-positive samples were incorrectly classified as negative. These misclassifications are likely due to very low concentrations of the CD63 biomarker, potentially falling near or below the lower detection limit of the sensor. Additionally, sensor sensitivity variation and sample degradation during handling may have contributed to this outcome. In contrast, for the false positives instances, where healthy samples were incorrectly classified as cancerous, were rare as reflected in the 100% precision of the Random Forest model for CV. This indicates that all predicted positives were indeed true positives. For SWV, although precision slightly dropped to 86.4%, the model still demonstrated a balanced classification capability, misclassifying only a small number of healthy samples. This is likely due to non-specific current peaks close to the threshold caused by background noise or to biological variability in the control samples or minor contamination during sample preparation.

The clinical application of any diagnostic tool, including the proposed biosensor system, necessitates a careful consideration of false positive and false negative results. A false positive result, indicating healthy sample predicted as cancerous, could lead to unnecessary psychological stress for the patient, additional invasive testing, and increased healthcare costs. Conversely, a false negative, indicating cancerous sample predicted as healthy, poses an even greater risk by delaying diagnosis and treatment, which is especially detrimental in diseases like lung cancer where early detection is crucial for survival. In a clinical setting, our biosensor is envisioned as a rapid, point-of-care screening tool. Positive results from the biosensor would ideally be followed by confirmatory tests such as CT scans and biopsies, to ensure accurate diagnosis. Conversely, negative results could help in ruling out lung cancer in low-risk individuals, reducing the burden on conventional diagnostic pathways.

The trained random forest model was integrated into the developed biosensor platform to provide real-time analysis of the experimental data. This integration enables a rapid and automated interpretation of the biosensor responses, significantly reducing the time required for lung cancer biomarker detection.

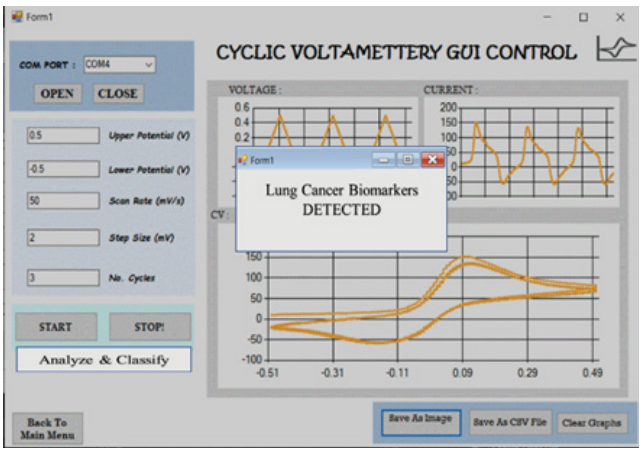

FIGURE 18. GUI interface: detected lung cancer CD63 biomarkers.

Figure 18 presents the classification results that has been integrated into the software application interface. User may access the model by clicking the "Analyze and Classify" button. Prior to being entered into the model, the experimental data seen in the GUI undergoes a preprocessing. As can be seen from Figure 18, a pop-up window will be shown to the user to indicate the results of the CD63 protein lung cancer biomarker detection. Using the machine learning model predictive capabilities, it can classify and identify the presence and absence of the CD63 protein lung cancer biomarker.

V. LIMITATION AND FUTURE WORK

While the developed wireless electrochemical biosensor system demonstrates promising capabilities for CD63 protein

detection, it is worth noting certain limitations that will be taken into consideration for the future works. One of the constraints is the relatively small dataset, which is primarily due to the early-stage nature of this research and since this study represents one of the first implementations of CD63 detection using a fully integrated electrochemical biosensor platform with machine learning and wireless communication, there were no existing datasets available for model training or benchmarking. All data used in this study were exclusively collected using the developed biosensor system, ensuring high data integrity but also highlighting the need for further large-scale validation. Secondly, this study focused exclusively on the CD63 protein as a biomarker for lung cancer. While CD63 is a well-established EV marker, it is not a lung cancer-specific marker. The protein is expressed on EVs originating from various cell types and disease states, which may compromise the biosensor's specificity and sensitivity. Future work should incorporate a multiplexed sensing strategy capable of detecting several lung cancer-specific biomarkers to improve accuracy and specificity. Finally, the current study did not evaluate the potential impact of biological sample matrices on the biosensor's performance. Liquid biopsy samples like blood are complex and contain many other biomolecules like albumin which can foul sensor surfaces and interfere with signal detection. Thus, assessing the selectivity of the biosensor in the presence of these endogenous biomolecules and additional lung cancer markers is crucial to simulate clinical conditions and determine cross-reactivity. Addressing these limitations in future research will be critical for advancing the platform toward practical implementation in routine clinical diagnostics. The system is powered by a 9V 600 mAh battery, supporting up to 8 hours of continuous operation. Power profiling revealed that Bluetooth transmission is the most energy-intensive process, with peak currents around 90 mA. Nonetheless, the current design is well-suited for prototype testing and short-term field applications. Future works could further improve energy efficiency by exploring rechargeable lithium-ion batteries with solar or energy harvesting options.

VI. CONCLUSION

In this work, a portable wireless electrochemical biosensor potentiostat platform for the detection of CD63 protein lung cancer biomarkers is developed. The developed device enables real-time visualization and complete transmission of the measurement electrochemical results into user's Firebase cloud. The performance of the proposed system was evaluated in terms of sensitivity, linearity and accuracy compared to a bench-top commercial instrument for two commonly used electrochemical techniques, namely, CV, SWV. Results show a decent potential for the detection of a CD63 protein lung cancer biomarkers in which the platform detects particles as low as 2×10^1 particles/mL. Its sensitivity is 5.188 μA per log unit concentration (particles/mL), which is considered decent compared to a commercial uStat8000 potentiostat lab-based platform. Random forest machine learning model integrated into the platform performs well with accuracy of 83.5% and 87.5% for the CV and SWV data, respectively. The developed portable potentiostat platform is a potential tool for point-of-care lung cancer diagnostic in a resource limited setting.

ACKNOWLEDGMENT

The authors would like to thank Dr. Leong Kok Hoong (Faculty of Pharmacy, Universiti Malaya) for the generous donation of A549 cells, Yeoh Hao Ing for her assistance with EV collection, and Dr. How Chee Wun (School of Pharmacy, Monash University Malaysia) for providing access to the NanoSight NS300 equipment.

REFERENCES

[1] *Global Cancer Burden Growing, Amidst Mounting Need for Services*, World Health Organization, Geneva, Switzerland, 2022.
[2] J. Y. Chang, "Stereotactic ablative radiotherapy versus lobectomy for operable stage I non-small-cell lung cancer: A pooled analysis of two randomised trials," *Lancet Oncol.*, vol. 16, no. 6, pp. 630–637, Jun. 2015.
[3] *Lung Cancer*, International Agency for Research on Cancer (IARC), Lyon, France, 2022.
[4] T. R. Church, W. C. Black, D. R. Aberle, C. D. Berg, K. L. Clingan, F. Duan, R. M. Fagerstrom, I. F. Gareen, D. S. Gierada, G. C. Jones, I. Mahon, P. M. Marcus, J. D. Sicks, A. Jain, and S. E. Baum, "Results of initial low-dose computed tomographic screening for lung cancer," *New England J. Med.*, vol. 368, no. 21, pp. 1980–1991, 2013.
[5] D. Liu, J. Wang, L. Wu, Y. Huang, Y. Zhang, M. Zhu, Y. Wang, Z. Zhu, and C. Yang, "Trends in miniaturized biosensors for point-of-care testing," *TrAC Trends Anal. Chem.*, vol. 122, Jan. 2020, Art. no. 115701.
[6] M. Caux, A. Achit, K. Var, G. Boitel-Aullen, D. Rose, A. Aubouy, S. Argentieri, R. Campagnolo, and E. Maisonhaute, "PassStat, a simple but fast, precise and versatile open source potentiostat," *HardwareX*, vol. 11, Apr. 2022, Art. no. e00290.
[7] A. Singh, A. Sharma, A. Ahmed, A. K. Sundramoorthy, H. Furukawa, S. Arya, and A. Khosla, "Recent advances in electrochemical biosensors: Applications, challenges, and future scope," *Biosensors*, vol. 11, no. 9, p. 336, Sep. 2021.
[8] A. Ainla, M. P. S. Mousavi, M.-N. Tsaloglou, J. Redston, J. G. Bell, M. T. Fernández-Abedul, and G. M. Whitesides, "Open-source potentiostat for wireless electrochemical detection with smartphones," *Anal. Chem.*, vol. 90, no. 10, pp. 6240–6246, May 2018.
[9] M. R. A. Wahab, T. Palaniyandi, M. Ravi, S. Viswanathan, G. Baskar, H. Surendran, S. G. D. Gangadharan, and B. K. Rajendran, "Biomarkers and biosensors for early cancer diagnosis, monitoring and prognosis," *Pathol. Res. Pract.*, vol. 250, Oct. 2023, Art. no. 154812.
[10] J. Wang, B. Xu, L. Shi, L. Zhu, and X. Wei, "Prospects and challenges of AI and neural network algorithms in MEMS microcantilever biosensors," *Processes*, vol. 10, no. 8, p. 1658, Aug. 2022.
[11] X. Jin, C. Liu, T. Xu, L. Su, and X. Zhang, "Artificial intelligence biosensors: Challenges and prospects," *Biosensors Bioelectron.*, vol. 165, Oct. 2020, Art. no. 112412.
[12] Y. Zhao, H. Zhang, Y. Li, X. Yu, Y. Cai, X. Sha, S. Wang, Z. Zhan, J. Xu, and L. Liu, "AI powered electrochemical multi-component detection of insulin and glucose in serum," *Biosensors Bioelectron.*, vol. 186, Aug. 2021, Art. no. 113291.
[13] S. Park, H. Kang, Y. Choi, S. G. Yoon, H. J. Park, H. Jin, H. Kim, Y. Jeong, J. S. Shim, T. I. Noh, S. H. Kang, and K. H. Lee, "Precision screening with sequential multi-algorithm reclassification technique (SMART): Saving bladders from unnecessary cystectomy," *Comput. Biol. Med.*, vol. 189, May 2025, Art. no. 109980.
[14] Z. Xing, G. Ma, L. Wang, L. Yang, X. Guo, and S. Chen, "Toward visual interaction: Hand segmentation by combining 3-D graph deep learning and laser point cloud for intelligent rehabilitation," *IEEE Internet Things J.*, vol. 12, no. 12, pp. 21328–21338, Jun. 2025.

[15] Z. Xing, Z. Meng, G. Zheng, G. Ma, L. Yang, X. Guo, L. Tan, Y. Jiang, and H. Wu, "Intelligent rehabilitation in an aging population: Empowering human-machine interaction for hand function rehabilitation through 3D deep learning and point cloud," *Frontiers Comput. Neurosci.*, vol. 19, pp. 1–3, May 2025.

[16] D. Andersson, M. Kubista, and A. Ståhlberg, "Liquid biopsy analysis in cancer diagnostics," *Mol. Aspects Med.*, vol. 72, Apr. 2020, Art. no. 100839.

[17] A. Mohan, S. Agarwal, M. Clauss, N. S. Britt, and N. K. Dhillon, "Extracellular vesicles: Novel communicators in lung diseases," *Respiratory Res.*, vol. 21, no. 1, p. 175, Jul. 2020.

[18] Q. Zhou, A. Rahimian, K. Son, D.-S. Shin, T. Patel, and A. Revzin, "Development of an aptasensor for electrochemical detection of exosomes," *Methods*, vol. 97, pp. 88–93, Mar. 2016.

[19] Z. Altintas and I. Tothill, "Biomarkers and biosensors for the early diagnosis of lung cancer," *Sens. Actuators B, Chem.*, vol. 188, pp. 988–998, Nov. 2013.

[20] J. Su, S. Chen, Y. Dou, Z. Zhao, X. Jia, X. Ding, and S. Song, "Smartphone-based electrochemical biosensors for directly detecting serum-derived exosomes and monitoring their secretion," *Anal. Chem.*, vol. 94, no. 7, pp. 3235–3244, Feb. 2022.

[21] J. Zhang, L.-L. Wang, M.-F. Hou, Y.-K. Xia, W.-H. He, A. Yan, Y.-P. Weng, L.-P. Zeng, and J.-H. Chen, "A ratiometric electrochemical biosensor for the exosomal microRNAs detection based on bipedal DNA walkers propelled by locked nucleic acid modified toehold mediate strand displacement reaction," *Biosensors Bioelectron.*, vol. 102, pp. 33–40, Apr. 2018.

[22] S. Jeong, J. Park, D. Pathania, C. M. Castro, R. Weissleder, and H. Lee, "Integrated magneto–electrochemical sensor for exosome analysis," *ACS Nano*, vol. 10, no. 2, pp. 1802–1809, Feb. 2016.

[23] S. L. Moura, C. G. Martín, M. Martí, and M. I. Pividori, "Multiplex detection and characterization of breast cancer exosomes by magneto-actuated immunoassay," *Talanta*, vol. 211, May 2020, Art. no. 120657.

[24] A. Prasad, K. Mahato, P. K. Maurya, and P. Chandra, "Biomaterials for biosensing applications," *J Anal Bioanal Tech*, vol. 7, no. 2, p. 1000, 2016.

[25] B. Cai, S. Wang, L. Huang, Y. Ning, Z. Zhang, and G.-J. Zhang, "Ultrasensitive label-free detection of PNA–DNA hybridization by reduced graphene oxide field-effect transistor biosensor," *ACS Nano*, vol. 8, no. 3, pp. 2632–2638, Mar. 2014.

[26] M. M. Barsan, M. E. Ghica, and C. M. A. Brett, "Electrochemical sensors and biosensors based on redox polymer/carbon nanotube modified electrodes: A review," *Analytica Chim. Acta*, vol. 881, pp. 1–23, Jun. 2015.

[27] M. D. M. Dryden and A. R. Wheeler, "DStat: A versatile, open-source potentiostat for electroanalysis and integration," *PLoS ONE*, vol. 10, no. 10, Oct. 2015, Art. no. e0140349.

[28] W.-J. Ma, C.-H. Luo, J.-L. Lin, S.-H. Chou, P.-H. Chen, M.-J. Syu, S.-H. Kuo, and S.-C. Lai, "A portable low-power acquisition system with a urease bioelectrochemical sensor for potentiometric detection of urea concentrations," *Sensors*, vol. 16, no. 4, p. 474, Apr. 2016.

[29] S. Wang, J. Zhang, O. Gharbi, V. Vivier, M. Gao, and M. E. Orazem, "Electrochemical impedance spectroscopy," *Annu. Rev. Anal. Chem.*, vol. 1, no. 1, pp. 207–229, 2021.

[30] A. Sun, A. G. Venkatesh, and D. A. Hall, "A multi-technique reconfigurable electrochemical biosensor: Enabling personal health monitoring in mobile devices," *IEEE Trans. Biomed. Circuits Syst.*, vol. 10, no. 5, pp. 945–954, Oct. 2016.

[31] D. Pletcher, "Analytical electrochemistry," *Angew. Chemie-English Ed.*, vol. 385, no. 2, p. 283, 1995.

[32] M. Li, Y.-T. Li, D.-W. Li, and Y.-T. Long, "Recent developments and applications of screen-printed electrodes in environmental assays—A review," *Analytica Chim. Acta*, vol. 734, pp. 31–44, Jul. 2012.

[33] C. Loncaric, Y. Tang, C. Ho, M. A. Parameswaran, and H.-Z. Yu, "A USB-based electrochemical biosensor prototype for point-of-care diagnosis," *Sens. Actuators B, Chem.*, vol. 161, no. 1, pp. 908–913, Jan. 2012.

[34] Y. Cao, J. Xia, L. Li, Y. Zeng, J. Zhao, and G. Li, "Electrochemical biosensors for cancer diagnosis: Multitarget analysis to present molecular characteristics of tumor heterogeneity," *JACS Au*, vol. 4, no. 12, pp. 4655–4672, Dec. 2024.

[35] Y. Zhao, "Application of electrochemical ELISA in cancer detection," in *Biological Sciences and Environmental Health*. CRC Press, Nov. 2024, pp. 263–269, doi: 10.1201/9781003587590-38.

[36] S. Sakib, K. Bajaj, P. Sen, W. Li, J. Gu, Y. Li, and L. Soleymani, "Comparative analysis of machine learning algorithms used for translating aptamer-antigen binding kinetic profiles to diagnostic decisions," *ACS Sensors*, vol. 10, no. 2, pp. 907–920, Feb. 2025.

[37] C. M. Singhal, V. Kaushik, A. Awasthi, J. B. Zalke, S. Palekar, P. Rewatkar, S. K. Srivastava, M. B. Kulkarni, and M. L. Bhaiyya, "Deep learning-enhanced portable chemiluminescence biosensor: 3D-printed, smartphone-integrated platform for glucose detection," *Bioengineering*, vol. 12, no. 2, p. 119, Jan. 2025.

[38] V. N. Palakollu, Y. V. M. Reddy, M. I. Shekh, S. V. P. Vattikuti, J. Shim, and R. Karpoormath, "Electrochemical immunosensing of tumor markers," *Clinica Chim. Acta*, vol. 557, Apr. 2024, Art. no. 117882.

[39] L. Fu and H. Karimi-Maleh, "Leveraging electrochemical sensors to improve efficiency of cancer detection," *World J. Clin. Oncol.*, vol. 15, no. 3, pp. 360–373, Mar. 2024.

[40] Z. Huang, Y. Li, V. Bucci, and J. P. Haran, "Decoding cancer prognosis with deep learning: The ASD-cancer framework for tumor microenvironment analysis," *mSystems*, vol. 10, no. 5, May 2025, Art. no. e0145524.

[41] A. Arora and K. K. Yadav, "Potentiometric devices for biomarkers," in *Sensing Materials and Devices for Biomarkers*, 2024, pp. 146–165, doi: 10.1039/9781837673230-00146.

[42] C.-A. Wang, Y.-C. Hou, Y.-K. Hong, Y.-J. Tai, C. Shen, P.-C. Hou, J.-L. Fu, C.-L. Wu, S. M. Cheng, D.-Y. Hwang, Y.-Y. Su, Y.-S. Shan, and S.-J. Tsai, "Intercellular TIMP-1-CD63 signaling directs the evolution of immune escape and metastasis in KRAS-mutated pancreatic cancer cells," *Mol. Cancer*, vol. 24, no. 1, p. 42, Jan. 2025.

[43] N. Praween, P. G. K. Thej, and P. K. Basu, "Electric field-induced exosome lysis and quantification of TSG101-derived protein via electrochemical sensing," *IEEE Sensors Lett.*, vol. 9, no. 2, pp. 1–4, Feb. 2025.

[44] M. Li, P. Yang, J. Wu, R. Ni, H. Yuan, Z. Guo, J. Zou, W. Gao, H. Cong, and Q. Jin, "Highly efficient and label-free sensitive detection of tumor-derived exosome with an aptasensor-based microfluidic chip," *Microchemical J.*, vol. 203, Aug. 2024, Art. no. 110875.

[45] A. Javed, N. Kong, M. Mathesh, W. Duan, and W. Yang, "Nanoarchitectonics-based electrochemical aptasensors for highly efficient exosome detection," *Sci. Technol. Adv. Mater.*, vol. 25, no. 1, p. 5, Dec. 2024.

[46] *Sensit Smart [Potentiostat]*, PalmSens, Utrecht, The Netherlands, 2023.

[47] *PalmSens [Potentiostat]*, PalmSens, Utrecht, The Netherlands, 2023.

[48] *Stat-I 400 [Potentiostat]*, Metrohm, Herisau, Switzerland, 2023.

[49] *CS100E [Potentiostat]*, Corrtest Instruments, Wuhan, China, 2023.

[50] A. A. Rowe, A. J. Bonham, R. J. White, M. P. Zimmer, R. J. Yadgar, T. M. Hobza, J. W. Honea, I. Ben-Yaacov, and K. W. Plaxco, "CheapStat: An open-source, 'do-it-yourself' potentiostat for analytical and educational applications," *PLoS ONE*, vol. 6, no. 9, Sep. 2011, Art. no. e23783.

[51] A. Scott, R. Pandey, S. Saxena, E. Osman, Y. Li, and L. Soleymani, "A smartphone operated electrochemical reader and actuator that streamlines the operation of electrochemical biosensors," *ECS Sensors Plus*, vol. 1, no. 1, Mar. 2022, Art. no. 014601.

[52] M. W. Glasscott, M. D. Verber, J. R. Hall, A. D. Pendergast, C. J. McKinney, and J. E. Dick, "SweepStat: A build-it-yourself, two-electrode potentiostat for macroelectrode and ultramicroelectrode studies," *J. Chem. Educ.*, vol. 97, 2019. [Online]. Available: https://doi.org/10.1021/acs.jchemed.9b00893

[53] O. S. Hoilett, J. F. Walker, B. M. Balash, N. J. Jaras, S. Boppana, and J. C. Linnes, "KickStat: A coin-sized potentiostat for high-resolution electrochemical analysis," *Sensors*, vol. 20, no. 8, p. 2407, Apr. 2020.

[54] P. Irving, R. Cecil, and M. Z. Yates, "MYSTAT: A compact potentiostat/galvanostat for general electrochemistry measurements," *HardwareX*, vol. 9, Apr. 2021, Art. no. e00163.

[55] D. M. Jenkins, B. E. Lee, S. Jun, J. Reyes-De-Corcuera, and E. S. McLamore, "ABE-stat, a fully open-source and versatile wireless potentiostat project including electrochemical impedance spectroscopy," *J. Electrochemical Soc.*, vol. 166, no. 9, pp. B3056–B3065, 2019.

[56] P. Lopin and K. V. Lopin, "PSoC-stat: A single chip open source potentiostat based on a programmable system on a chip," *PLoS ONE*, vol. 13, no. 7, Jul. 2018, Art. no. e0201353.

[57] S. Sarkar and M. Bhattacharya, "SStat: Wi-Fi and Bluetooth integrated multimodal 'do-it-yourself' electrochemical potentiostat," in *Proc. IECON 46th Annu. Conf. IEEE Ind. Electron. Soc.*, Oct. 2020, pp. 5249–5254.

[58] *Rodeostat [Potentiostat]*, IO Rodeo, Pasadena, CA, USA, 2023.

[59] L. Stratmann, B. Heery, and B. Coffey, "EmStat pico: Embedded electrochemistry with a miniaturized, software-enabled, potentiostat system on module," Analog Devices, Inc., Tech. Rep., 2019. [Online]. Available: https://www.analog.com/en/resources/technical-articles/emstat-pico-embedded-electrochemistry-with-a-miniaturized-software-enabled-potentiostat-system-on-mo.html
[60] S. D. Adams, E. H. Doeven, K. Quayle, and A. Z. Kouzani, "MiniStat: Development and evaluation of a mini-potentiostat for electrochemical measurements," *IEEE Access*, vol. 7, pp. 31903–31912, 2019.
[61] E. W. Brown, M. W. Glasscott, K. Conley, J. Barr, J. D. Ray, L. C. Moores, and A. Netchaev, "ACEstat: A DIY guide to unlocking the potential of integrated circuit potentiostats for open-source electrochemical analysis," *Anal. Chem.*, vol. 94, no. 12, pp. 4906–4912, Mar. 2022.
[62] J. P. de Campos da Costa, W. B. Bastos, P. I. da Costa, M. A. Zaghete, E. Longo, and J. P. Carmo, "Portable laboratory platform with electrochemical biosensors for immunodiagnostic of hepatitis C virus," *IEEE Sensors J.*, vol. 19, no. 22, pp. 10701–10709, Nov. 2019.
[63] K. Krorakai, S. Klangphukhiew, S. Kulchat, and R. Patramanon, "Smartphone-based NFC potentiostat for wireless electrochemical sensing," *Appl. Sci.*, vol. 11, no. 1, p. 392, Jan. 2021.
[64] V. Bianchi, A. Boni, S. Fortunati, M. Giannetto, M. Careri, and I. De Munari, "A Wi-Fi cloud-based portable potentiostat for electrochemical biosensors," *IEEE Trans. Instrum. Meas.*, vol. 69, no. 6, pp. 3232–3240, Jun. 2020.
[65] S. S. Low, Y. Pan, D. Ji, Y. Li, Y. Lu, Y. He, Q. Chen, and Q. Liu, "Smartphone-based portable electrochemical biosensing system for detection of circulating microRNA-21 in saliva as a proof-of-concept," *Sens. Actuators B, Chem.*, vol. 308, Apr. 2020, Art. no. 127718.
[66] T. Akagi, K. Kato, M. Kobayashi, N. Kosaka, T. Ochiya, and T. Ichiki, "On-chip immunoelectrophoresis of extracellular vesicles released from human breast cancer cells," *PLoS ONE*, vol. 10, no. 4, pp. 1–13, Apr. 2015.
[67] F. N. Faruqu, L. Xu, and K. T. Al-Jamal, "Preparation of exosomes for siRNA delivery to cancer cells," *J. Visualized Experiments*, vol. 142, no. 142, Dec. 2018, Art. no. 3791.
[68] C. Théry, "Minimal information for studies of extracellular vesicles 2018 (MISEV2018): A position statement of the international society for extracellular vesicles and update of the MISEV2014 guidelines," *J. Extracellular Vesicles*, vol. 7, no. 1, Dec. 2018, Art. no. 1535750.
[69] S. R. Kumal, R. Kobayashi, S. Ueno, and T. Ichiki, "Photo-assisted fabrication of ribosome display microarray," *J. Photopolymer Sci. Technol.*, vol. 27, no. 4, pp. 459–465, 2014.
[70] M. Jarczewska, J. Rębiś, Ł. Górski, and E. Malinowska, "Development of DNA aptamer-based sensor for electrochemical detection of C-reactive protein," *Talanta*, vol. 189, pp. 45–54, Nov. 2018.
[71] Q. Yu, Q. Zhao, S. Wang, S. Zhao, S. Zhang, Y. Yin, and Y. Dong, "Development of a lateral flow aptamer assay strip for facile identification of theranostic exosomes isolated from human lung carcinoma cells," *Anal. Biochemistry*, vol. 594, Apr. 2020, Art. no. 113591.
[72] M. Ruzycka-Ayoush, A. M. Nowicka, A. Kowalczyk, A. Gluchowska, A. Targonska, G. Mosieniak, K. Sobczak, M. Donten, and I. P. Grudzinski, "Exosomes derived from lung cancer cells: Isolation, characterization, and stability studies," *Eur. J. Pharmaceutical Sci.*, vol. 181, Feb. 2023, Art. no. 106369.

AHMED FAOZI RABEA received the B.Eng. degree in electrical and electronic engineering from Universiti Putra Malaysia, Selangor, Malaysia. Currently, he is pursuing the M.Eng.Sc. degree in engineering and engineering trades (electronics and automation), focusing on bioinstrumentation with Universiti Malaya, Malaysia. His research interests include biomedical instrumentation, signal processing, digital system design, embedded systems, and the integration of the Internet of Things (IoT) and machine learning technologies for healthcare, environmental monitoring, and smart sensing applications.

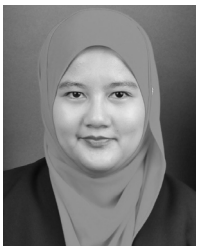

EFFARIZA HANAFI (Senior Member, IEEE) received the B.Eng. degree (Hons.) in telecommunications from the University of Adelaide, Adelaide, SA, Australia, in 2010, and the Ph.D. degree in electrical and electronic engineering from the University of Canterbury, Christchurch, New Zealand, in 2014. She joined the Universiti Malaya, Kuala Lumpur, Malaysia, where she is currently a Senior Lecturer at the Faculty of Engineering. She has authored and co-authored journal articles in ISI-indexed publications and refereed conference papers. Her main research interests include wireless communications, machine learning in wireless communications, the Internet of Things, cognitive radio, and 5G networks and beyond. In 2015, she was a recipient of the Universiti Malaya Excellence Awards. She is a Chartered Engineer of the Engineering Council U.K.

SUBHASHINI RAJ KUMAL received the B.Sc. degree (Hons.) in applied chemistry from Universiti Malaya, Malaysia, in 2009, and the Ph.D. degree in bioengineering from The University of Tokyo, Japan, in 2016. She joined Universiti Malaya as a Research Assistant, in 2020, and was appointed as a Postdoctoral Research Fellow, in 2022. She has authored and co-authored peer-reviewed publications and is the co-inventor on patents related to biosensing. Her research interests include BioMEMS, molecular bioengineering and biosensors for biotechnology, and healthcare applications.

ANIS SALWA MOHD KHAIRUDDIN (Member, IEEE) received the Bachelor of Electrical Engineering degree from Universiti Tenaga Nasional, Malaysia, in 2008, the Master of Computer Engineering degree from the Royal Melbourne Institute of Technology (RMIT), Australia, in 2010, and the Ph.D. degree in electrical engineering from Universiti Teknologi Malaysia, in 2014. She is currently an Associate Professor at the Department of Electrical Engineering, Faculty of Engineering, Universiti Malaya, Malaysia. Her research interests include intelligent systems and pattern recognition.

LEO BEY FEN received the Ph.D. degree from London Centre for Nanotechnology, Imperial College London, U.K. She is currently an Associate Professor at the Faculty of Medicine, University of Malaya (UM), and a Research Fellow at the Nanotechnology and Catalysis Research Centre, UM. Her research primarily focuses on nanomaterials synthesis and characterization, and creating portable, rapid, and sensitive point-of-care devices for biomedical applications. Her work has been recognized with numerous peer-reviewed articles published in high-impact journals. Her impactful contributions are evident in her extensive publication record, with over 90 scientific articles and book chapters, garnering more than 3000 citations and an H-index of 32. Her team's biosensor is receiving prestigious awards, including the Gold Award at the International Conference and Exposition on Inventions by the Institutions of Higher Learning. She serves as a reviewer for several prestigious scientific publications and is actively involved in standardization efforts, including serving as a technical committee member for the ISO/TC 229 Standard and OECD certification related to nanomaterials.